Thermal Science and Engineering 2024, 7(3), 8615.
https://doi.org/10.24294/tse.v7i3.8615

Article

Analysis of magnetized bio-convective Ellis nanofluid flow: Impact of viscous dissipation and activation energy

Tayyaba Akhtar[1,*], Muhammad Abid[2], Mohamed M. Awad[3], Munaza Chaudhry[1], Muhammad Imran[1]

[1] Department of Mathematics, Government College University Faisalabad, Faisalabad 38000, Pakistan
[2] Department of Mathematics, North Caroline State University, 27695 NC Raleigh, USA
[3] Mechanical Power Engineering Department, Faculty of Engineering, Mansoura University, Mansoura, Egypt
*** Corresponding author:** Tayyaba Akhtar, tayyabakanwal10@gmail.com

CITATION

Akhtar T, Abid M, Awad MM, et al. Analysis of magnetized bio-convective Ellis nanofluid flow: impact of viscous dissipation and activation energy. Thermal Science and Engineering. 2024; 7(3): 8615. https://doi.org/10.24294/tse.v7i3.8615

ARTICLE INFO

Received: 5 May 2024
Accepted: 26 June 2024
Available online: 8 July 2024

COPYRIGHT

Copyright © 2024 by author(s). *Thermal Science and Engineering* is published by EnPress Publisher, LLC. This work is licensed under the Creative Commons Attribution (CC BY) license. https://creativecommons.org/licenses/by/4.0/

Abstract: This study delves into the complex flow dynamics of magnetized bioconvective Ellis nanofluids, highlighting the critical roles of viscous dissipation and activation energy. By employing a MATLAB solver to tackle the boundary value problem, the research offers a thorough exploration of how these factors, along with oxytactic microorganism's mobility, shape fluid behavior in magnetized systems. Our findings demonstrate that an increase in the magnetization factor (M) leads to a decrease in both velocity and temperature due to enhanced interparticle resistance from the Lorentz force. Additionally, streamline analysis reveals that higher mixed convection parameters (א) intensify flow concentration near surfaces, while increased slip parameters reduce shear stress and boundary layer thickness. Although isotherm analysis shows that higher Ellis fluid parameters enhance heat conduction, with greater porosity values promoting efficient thermal dissipation. These insights significantly advance our understanding of nanofluid dynamics, with promising implications for bioengineering and materials science, setting the stage for future research in this field.

Keywords: Ellis nanofluid; activation energy; darcy-forchheimer; magnetic field; numerical scheme

1. Introduction

Nanotechnology is an area of applied sciences and technology that includes atomic and molecular-scale manipulation of matter, usually below 100 nanometers. So, unlike their macroscale equivalents, these materials have special features because of the elevated surface-to-volume ratio and other novel physiochemical properties such as solubility, strength, diffusivity, magnetic, thermodynamic, etc. At present, various industries use fluids to increase production by increasing/reducing the flow of energy to the system. In this regard, nanofluids are of great significance. Nanofluids consist of sparse liquid suspensions of nanoparticles. Previous research suggests that nanofluids exhibit superior thermophysical properties. Contrasted with base fluids such as oil or water, nanofluids exhibit enhanced properties entailing thermal characteristics, thermal diffusivity, viscosity, and convective heat transfer coefficients. Typically, nanoliquids utilize nanomaterials derived from metals (such as Ag, Al, Cu, Fe, Au), non-metals (including carbon nanotubes and graphite), metallic oxides (like Al_2O_3, CuO, TiO_2, SiO_2, FeO), carbides/nitrides (such as TiC, SiC, TiN, SiN, AlNC, AlN), and layered materials (e.g., Al + Al_2O_3, Cu + C), with conventional liquids like water, glycol, and engine oil commonly employed as base fluids in the nanofluid formation process.

The development of nanotechnology has significantly enhanced modern living.

Owing to the beneficial use of nanoparticles, we have seen their valuable applications span across the disciplines of engineering, chemistry, mechanics, and biology. Nanoparticles are employed to enhance cooling in diverse heat exchange processes, including metal strip cooling, chemical transformations, automobile engines, welding machinery, microwave tubes, nuclear reactions, computing devices, and assorted engineering equipment, owing to their enhanced thermal characteristics [1]. In another article, Turkyilmazoglu [2] explored the thermal behavior of nanofluid flow in a wall jet employing five distinct nanoparticle varieties. He aimed to figure out how different nanofluids affect the heat and flow behavior of the wall jet. Arafa et al. [3] conducted a study on entropy generation in nanofluid flow with changing porosity along complex vertical duct. It has been noted that using nanoparticles results in very good improvement. It has been noted that the application of nanoparticles results in remarkable improvement. A comparable estimated resolution for fully established nanofluid flow is derived in Hussain et al.'s paper [4]. For the examination of heat and mass transfer phenomena, a vertical conduit with composite permeable medium has been used. A few significant studies on nanofluids are mentioned in Abbas et al. [5], Nadeem et al. [6], and Amjad et al.'s [7] works. In the comprehensive work, the authors delve into advanced mathematical approaches for understanding the behavior of nanofluids and complex fluid systems [8]. This resource offers critical insights into various fluid dynamic models, emphasizing their practical applications in both theoretical and engineering contexts.

Since the classical Newtonian liquid hypothesis is unable to fully estimate the significance of fluid characteristics involving suspended molecules, non-Newtonian flow, and heat transfer processes, it has garnered considerable attention. Not only are non-Newtonian fluid flows valuable from a technological standpoint, but their governing equations also display interesting mathematical properties. The physicochemical properties of Newtonian fluids are incredibly complex, and there isn't a single constitutive relation that can be universally applied to all non-Newtonian fluids. In the articles by Yahya et al. [9], Ahmad et al. [10], Gul et al. [11], and Abdal et al. [12], a number of noteworthy studies on these flows have been presented. All of the aforementioned studies investigate the dynamics of flow, heat, and mass transfer of assorted non-Newtonian fluids through a comprehensive literature review. Nevertheless, there has been no endeavor to characterize the flow dynamics of magnetized bioconvective Ellis nanofluids while considering the ramifications of viscous dissipation and activation energy. The Bingham (viscoelastic) and Power law models are generalized by the Ellis model. At elevated shear stresses, it demonstrates power-law behavior, transitioning to Newtonian characteristics at lower shear forces. The constitutive equation of the Ellis model serves as a foundational framework for deducing the constitutive equation of the Bingham model. The Ellis fluid model approach is flexible in adjusting viscosity rheological data across various non-Newtonian fluids and geometries. Hence, the Ellis fluid pattern can be regarded as a fusion of the Bingham, power-law, and Newtonian fluid models. It offers a helpful infrastructure for assessing the rheology of various biofluids, including blood, chyme, pulmonary mucus, cervical mucus, etc. Furthermore, several notable studies have explored the application of the Ellis fluid model in plentiful designs for flow analysis [13–16].

Analyzing heat and mass transfer spectacles in fluid flow deformable cylinders has attracted significant attention in light of its relevance in engineering and industry. Shaheen et al. [17] explored the interaction between Soret and Dufour phenomena in the flow of Casson nanofluid around a deformable cylinder, considering dynamic properties and integrating Arrhenius activation energy. Hayat et al. [18] interrogated magnetohydrodynamic axisymmetric flow characteristics of a third-grade fluid adjacent to a stretching cylinder. Also, Grigoriadis et al. [19] ventured the MHD flow behavior around a cylindrical object employing the Immersed Boundary Method to comprehensively analyze the fluid dynamics. Anuar et al. [20] assessed how magnetohydrodynamics (MHD) affected the steady-state (2-D) mixed convection flow in carbon nanotubes that was caused by a nonlinear surface. When using carbon nanotubes of both single and multi-wall varieties (CNTs), kerosene and water are utilized as the base fluids. Ramesh et al. [21] presented a detailed computational analysis on radiative non-Newtonian Carreau nanofluid flow in a microchannel under magnetic properties. In an innovative study, Mebarek-Oudina et al. [22] explored the role of a quadratic linearly radiating heat source with Carreau nanofluid and exponential space-dependence past a cone and a wedge, highlighting its implications for medical engineering and renewable energy applications. Khan et al. [23] examined nonlinear radiation effects in magnetohydrodynamic flow around a cylinder containing chemically reactant species by using the shooting technique.

Understanding the swimming capability of oxytactic microorganisms is vital for elucidating various biological characteristics related to bioconvection. The dispersion of oxytactic swimming microorganisms in a constricted space is referred to as bioconvection. Bioconvection entails convective fluid motion at the nanoscale level brought on by the density gradient and the concurrent swimming of motile microorganisms. Furthermore, the use of microorganisms in fluid mechanics has increased recently in order to enhance heat transport while reducing nanoparticle agglomeration. Kuznetsov and Avramenko [24] and Geng and Kuznetsov [25] originally scrutinized bioconvection in the existence of nanoparticles. Afterwards, the concept of suspending nanoparticles with gyrotactic microorganisms was proposed by Kuznetsov [26], using Buongiorno's principle. Bég et al. [27] conducted numerical analysis regarding the bioconvection phenomenon of nanofluid flow through porous media. In a detailed study, Mebarek-Oudina et al. [28] investigated the hybrid nanofluid magneto-convective flow and the role of porous media in contributing to entropy generation. Dharmaiah et al. [29] numerically investigated the magnetic dipole effect on a radiative ferromagnetic liquid flowing over a porous stretched sheet that provides crucial insights into the interaction between magnetic fields and fluid flow dynamics.

Flow of bioconvection through symmetrical conduit infused with nanoparticles was considered by Akbar [30], and a bio-nano-engineering model was presented. The impetus of varying magnetic field on a model of blood clotting was also investigated by Bhatti et al. [31], employing the Jeffrey fluid model in conjunction with nanoparticles and microorganisms. Dharmaiah et al. [32] explored bio-convection phenomena within a slippery two-phase Maxwell nanofluid as it moves past a vertically induced magnetic stretching regime. This analysis is particularly

relevant to applications in biotechnology and engineering, where the interactions between magnetic fields and fluid dynamics play a crucial role. The magnetized laminar flow via a porous medium with non-Darcy flow characteristics of nanofluid and gyrotactic microorganisms was observed by Abbas and Palani [33]. The extrinsic magnetic effect and bioconvection flow were researched by Chakraborty et al. [34] with nanoparticles subjected to convective boundary conditions. Umar et al. [35] utilized the shooting technique to examine slip effects on a stretching sheet in fluid dynamics, considering 3-D Eyring-Powell fluid with activation energy. Incorporating the importance of gyrotactic microorganisms and thermal radiation, Khan et al. [36] discussed Oldroyd B fluid flow. This study employs a bioconvective flow of an Oldroyd-B nanofluid via stretching sheet undergoing oscillations. In the analysis of bioconvective electro-magnetohydrodynamics (EMHD) and dissipative Williamson nanofluid over a three-dimensional Riga plate, Akolade et al. [37] explored the effects of Joule heating in complex fluid flows. This study is pivotal for understanding how magnetic fields, heat dissipation, and fluid properties interact, particularly in industrial and technological applications. These phenomena are associated with several successful studies [38–41].

In a novel case study, Hiba et al. [42] conducted a thermal and streamline analysis in a grooved enclosure filled with Ag-MgO/water hybrid nanofluid using the Galerkin finite element method (FEM). The findings highlighted the potential of such nanofluids to enhance heat transfer efficiency in various engineering applications. In a significant work, Sharif and Mohammad [43] explored natural convection in cavities with constant flux heating at the bottom wall and isothermal cooling from the sidewalls. This study provided a comprehensive analysis of the thermal and flow patterns within such cavities. Based on the preceding studies, this paper aims to explore thermal and mass transfer properties within a steady, 2-dimensional MHD flow of Ellis nanofluid containing oxytactic microorganisms. The impact of thermal radiation, Darcy-Forchheimer, and magnetization via deformable cylinder are also covered in this study. The study employs the Buongiorno nanofluid model, integrating thermophoresis and Brownian motion phenomena.

Ellis nanofluid containing oxytactic microorganisms plays a crucial role in Thermal Science and Engineering by significantly enhancing heat transfer efficiency and thermal management across diverse applications. Its distinctive properties, coupled with the dynamic motion of microorganisms, facilitate improved convective heat transfer and lower thermal resistance. This advancement aligns with the journal's mission to further knowledge in thermal science, foster sustainable energy solutions, and investigate innovative materials that optimize thermal processes in engineering systems.

2. Model analysis

The characteristics of thermo-transfer within a steady, 2-dimensional magnetohydrodynamic (MHD) flow of Ellis nanofluid containing oxytactic microorganisms have been examined. This study also encompasses the impacts of magnetization, Darcy-Forchheimer, and radiative heat transfer over a deformable cylinder as depicted in **Figure 1**, subjected to boundary conditions tailored for

appropriate transport within the geometry. Consider $\bar{u}$ and $\bar{w}$ as the velocity aspects along the cylinder's horizontal $(z-axis)$ and radial $(r-axis)$ axes, respectively. The cylinder experiences stretching as described by the velocity equation $u_w(\bar{z}) = \frac{u_o \bar{z}}{L}$, where L represents the length of the cylinder and a is a constant value. A radial magnetic field B_o is imposed. The study employs the Buongiorno nanofluid model, incorporating Brownian motion and thermophoresis phenomena. Based on these considerations, the governing equations for the specified problems are as follows [44,45]:

$$\bar{u} \to 0, \bar{w} \to u_w, K_f \frac{\partial \bar{T}}{\partial \bar{r}} = -h_w(\bar{T}_w - \bar{T}), \bar{N} = \bar{N}_w$$

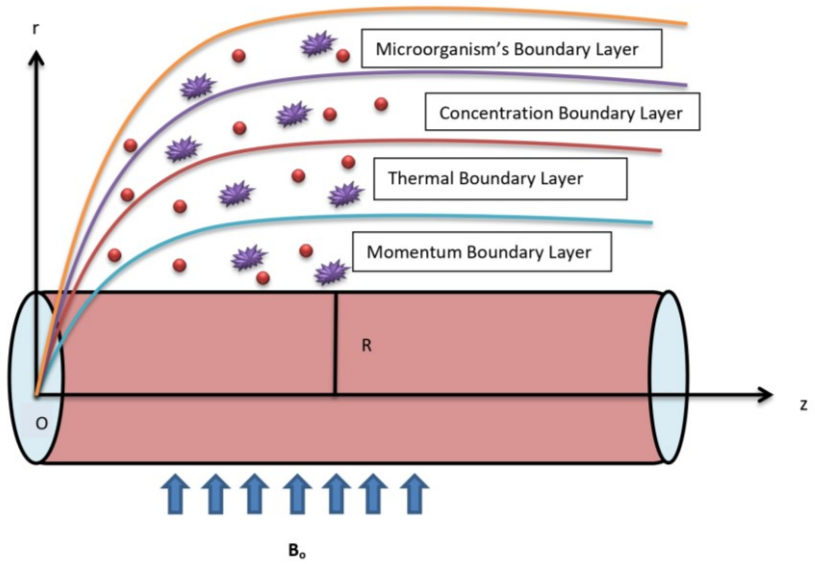

Figure 1. Visual depiction of the model's geometry.

$$\frac{\partial(r\bar{u})}{\partial \bar{z}} + \frac{\partial(r\bar{w})}{\partial \bar{r}} = 0 \tag{1}$$

$$\bar{u}\frac{\partial \bar{u}}{\partial \bar{z}} + \bar{w}\frac{\partial \bar{u}}{\partial \bar{r}} = \frac{1}{\rho_f}\frac{\partial}{\partial \bar{r}}\left(\frac{\bar{r}\mu_f}{1+\left(\frac{1}{\sqrt{2}\tau_o^2}\frac{\partial \bar{u}}{\partial \bar{z}}\right)^{\alpha-1}}\frac{\partial \bar{u}}{\partial \bar{r}}\right) - \frac{\sigma_f B_o^2 \bar{u}}{\rho_f} - \frac{\mu_f \bar{u}}{K^* \rho_f} - \frac{\sqrt{C}_b}{k^*}\bar{u}^2 + \frac{1}{\rho_f}[(1-C_\infty)\rho_f g\beta_t(\bar{T}-T_\infty) - (\rho_p - \rho_f)g\beta_c(\bar{C}-C_\infty) - (\rho_m - \rho_f)r^* g(\bar{N}-N_\infty)] \tag{2}$$

$$\bar{u}\frac{\partial \bar{T}}{\partial \bar{z}} + \bar{w}\frac{\partial \bar{T}}{\partial \bar{r}} = \frac{\alpha_f}{\bar{r}}\left(\frac{\partial \bar{T}}{\partial \bar{r}} + \bar{r}\frac{\partial^2 \bar{T}}{\partial \bar{r}^2}\right) + \tau\left[D_B\frac{\partial \bar{T}}{\partial \bar{r}}\frac{\partial \bar{C}}{\partial \bar{r}} + \frac{D_T}{T_\infty}\left(\frac{\partial \bar{T}}{\partial \bar{r}}\right)^2\right] + \frac{1}{(\rho C_p)_f}\frac{\partial}{\partial \bar{r}}\left(\frac{16\sigma *}{3kk^*}\bar{T}^3\frac{\partial \bar{T}}{\partial \bar{r}}\right) \tag{3}$$

$$\bar{u}\frac{\partial \bar{C}}{\partial \bar{z}} + \bar{w}\frac{\partial \bar{C}}{\partial \bar{r}} = \frac{D_T C_\infty}{T_\infty}\frac{\partial^2 \bar{T}}{\partial \bar{r}^2} + D_B\frac{\partial^2 \bar{C}}{\partial \bar{r}^2} - Kr^2\left(\frac{\bar{T}}{T_\infty}\right)^n exp\left(\frac{-E_a}{K_B \bar{T}}\right)(C_\infty - \bar{C}) \tag{4}$$

$$\bar{u}\frac{\partial \bar{N}}{\partial \bar{z}} + \bar{w}\frac{\partial \bar{N}}{\partial \bar{r}} = D_N\frac{\partial^2 \bar{N}}{\partial \bar{r}^2} - \frac{bW_c}{C_\infty}\frac{\partial}{\partial \bar{r}}\left(\bar{N}\frac{\partial \bar{C}}{\partial \bar{r}}\right) \tag{5}$$

The boundary conditions of problem typically match the configurations under investigation, as stated below:

$$\bar{r} = R,\ \bar{u} = 0,\ \ \bar{w} = u_w,\ \ k_f\frac{\partial \bar{T}}{\partial \bar{r}} = -h_w(T_w - \bar{T}),\ \ \bar{N} = N_w,\ \ D_B\left(\frac{\partial \bar{C}}{\partial \bar{r}}\right) + \frac{D_T}{T_\infty}\left(\frac{\partial \bar{T}}{\partial \bar{r}}\right) = 0, \tag{6}$$

$$\bar{r} \to \infty, \quad \bar{u} \to 0 \quad \bar{C} \to C_\infty, \quad \bar{T} \to T_\infty, \quad \bar{N} \to N_\infty$$

The provided similarity transformations below are employed.

$$\xi = \frac{r^2 - R^2}{2R}\sqrt{\frac{u_w}{z\mu_f}}, \; u = f'(\xi)\frac{zu_o}{L}, \; w = -\frac{R}{r}f(\xi)\sqrt{\frac{u_o\mu_f}{L}}$$
$$\theta(\xi) = \frac{T_\infty - \bar{T}}{T_\infty - T_w}, \; \phi(\xi) = \frac{C_\infty - \bar{C}}{C_\infty - C_w}, \; \chi(\xi) = \frac{N_\infty - \bar{N}}{N_\infty - N_w} \tag{7}$$

In Equation (7), ξ signifies the local transformation variable, $f'(\xi)$ represents the dimensionless velocity function, and $\theta(\xi)$ denotes the non-dimensionalized fluid temperature. Moreover, $\phi(\xi)$ represents the dimensionless volume fraction of nanoparticles, while $\chi(\xi)$ represents a motile microorganism lacking dimensional attributes. Equation (1) is identically satisfied. After the utilization of the above-mentioned transformation Equations (2)–(5), we got a subsequent scheme of ODEs.

$$\alpha(1+2\gamma\xi)[1+(2-\alpha)(\beta f'')^{\alpha-1}]f''' + \gamma[1+(2-\alpha)(\beta f'')^{\alpha-1}]f'' - [((1+\beta f'')^{\alpha-1})^2]Mf' - [(1 + \beta f'')^{\alpha-1}]^2\sigma_1 f' + [(1+\beta f'')^{\alpha-1}]^2[ff'' - F_r(f')^2 - (f')^2] + \aleph[\theta - N_r\phi - N_c\chi] \tag{8}$$

$$\frac{4}{3}Rd[(1+(\theta_w-1)\theta)^3](1+2\gamma\xi)\theta'' + 4Rd(\theta')^2[(1+(\theta_w-1)\theta)^2(\theta_w-1)] + 2\gamma\theta' + N_b\theta'\phi' + N_t(\theta')^2 + Prf\theta' = 0 \tag{9}$$

$$\phi'' + f'\phi' Le\frac{\xi}{2} + Lef\phi' + \frac{N_t}{N_b}(\theta'' + \gamma\theta') - Le\Omega(1+\Upsilon^*\theta)^n exp(\frac{-E}{1+\Upsilon^*\theta})\phi = 0 \tag{10}$$

$$\chi'' + Lb(f\chi' + \xi f'\chi) + Pe[\delta_1\phi' - (\gamma\delta_1 + \chi)\phi''] + Lb\chi'\phi = 0 \tag{11}$$

The subsequent boundary conditions are provided as:

When $\xi = 0;\; f(\xi) = 0,\; f'(\xi) = 1,$

$$\theta'(\xi) = -Bi[1-\theta(\xi)], \; \phi'(\xi) + \frac{N_t}{N_b}\theta'(\xi) = 0, \; \chi(\xi) = 1 \tag{12}$$

When $\xi \to 0; f'(\xi) \to 0,\; \theta(\xi) \to 0,\; \phi(\xi) \to 0,\; \chi(\xi) \to 0.$

Additionally, the dimensionless numbers and parameters within the above equations are as follows:

$$M = \frac{\sigma_f B_o^2 z}{\rho_f u_w}, F_r = \frac{C_b}{\sqrt{k^*}}, \gamma = \frac{1}{R}\sqrt{\frac{L\mu_f}{u_o}}, Rd = \frac{4\sigma T_\infty^3}{K^* k_f}, \beta = \sqrt{\frac{u_o^3 z^2 r^2}{2\tau_o^4 R^2 L^3 \mu_f}}, \sigma_1 = \frac{z\mu_f}{k^* u_w}, Bi = \frac{h_w}{k\mu_f}\sqrt{u_o^{-1}\nu_f}, Pr = \frac{\nu_f (C\rho)_f}{k_f}, N_r = \frac{\beta_c(C_\infty - C_w)(\rho_p - \rho_f)}{(1-C_\infty)(T_\infty - T_w)\beta_t \rho_f}, N_c = \frac{(\rho_m - \rho_f)\gamma^*(N_\infty - N_w)}{(1-C_\infty)(T_\infty - T_w)\beta_t\rho_f},$$
$$\aleph = \frac{G_{rt}}{Re_x^2}, G_{rt} = \frac{(1-C_\infty)\beta_t g(T_\infty - T_w)z^3}{2\nu_f^2}, Re_x^2 = \frac{u_w(z)}{\nu_f}, N_b = \frac{\tau D_B(C_\infty - C_w)}{\nu_f}, E = \frac{E_a}{K_B T_\infty}$$
$$N_t = \frac{\tau D_T(T_\infty - T_w)}{\nu_f T_\infty}, \theta_w = \frac{T_w}{T_\infty}, Le = \frac{\nu_f}{D_B}, \Omega = \frac{zkr^2r^2}{u_w R^2}, Lb = \frac{\mu_f}{D_N}, \delta_1 = \frac{N_\infty}{N_\infty - N_w}, \Upsilon^* = \frac{T_\infty - T_w}{T_\infty} \tag{13}$$

Here, M symbolizes the magnetic term, F_r is the Forchheimer number, γ represents the curvature parameter, Rd indicates the thermal radiation parameter, β signifies the Ellis fluid parameters, σ_1 denotes the porosity parameter, Bi stands for the thermal Biot number, Pr signifies the Prandtl number, and N_r represents the buoyancy force parameter. Bioconvection Rayleigh number N_c, $\aleph$ is the parameter for mixed convection, G_{rt} are the Grashof number, Re_x is the local Reynolds number, E activation energy parameter, N_t, θ_w, Le are the parameter of thermophoresis, temperature ratio parameter, Lewis number respectively. Furthermore, Ω represents the coefficient of chemical reaction, Lb stands for the bioconvection Lewis number, δ_1 denotes the parameter of bacterial concentration,

and Υ^* signifies the temperature gradient.

3. Physical quantities

3.1. Drag force acting on the surface

The skin friction coefficient is characterized as:

$$C_f = \frac{\tau_w}{\rho_f u_w^2} \tag{14}$$

where τ_w represents the apparent shear stress, defined as follows:

$$\tau_w = [\frac{\mu_f}{1 + (\frac{1}{\sqrt{2}\tau_o^2}\frac{\partial \bar{u}}{\partial z})^{\alpha-1}}\frac{\partial \bar{u}}{\partial z}]|_r = 0 \tag{15}$$

The provided similarity transformation enabled us to acquire:

$$C_f = Re_x^{\frac{-1}{2}}(\frac{f''(0)}{(1+\beta f'')^{\alpha-1}}) \tag{16}$$

3.2. The heat transfer rate

The Nusselt coefficient at a specific point is calculated as:

$$Nu_x = \frac{xq_m^*}{k_f(T_\infty - T_w)} \tag{17}$$

Therefore, the surface heat flux is expressed as:

$$q_m^* = -k_f(\frac{\partial \bar{T}}{\partial r})|_{r=0} - \frac{16\sigma^*}{3k^*}\bar{T}^3(\frac{\partial \bar{T}}{\partial r})|_{r=0} \tag{18}$$

The dimensionless form of the aforementioned equation is obtained by employing Equation (7) as follows:

$$Nu = -Re_x^{\frac{1}{2}}(1 + \frac{4}{3}Rd)\theta'(0) \tag{19}$$

3.3. Motile microorganisms

The quantity of motile microorganisms within the local density is described as:

$$Nn_x = \frac{xq_n}{D_N(N_\infty - N_w)} \tag{20}$$

where, motile microorganism flux defined as

$$q_n = -D_N\frac{\partial \bar{N}}{\partial r}|_{r=0} \tag{21}$$

The equation is expressed in its non-dimensionalized form as:

$$Nn = -Re_x^{\frac{1}{2}}\chi'(0) \tag{22}$$

4. Details of numerical procedure

Given the intricate nature of analytically solving ordinary differential equations (ODEs), we turn to numerical methods like the shooting method implemented through MATLAB's bvp4c software to tackle the governing equations. The core of bvp4c lies in its ability to transform the BVP into an IVP through the proposal of an initial solution. Numerous physical models involve nonlinear differential equations requiring numerical solutions, and the shooting method excels in achieving high

accuracy. This technique transforms boundary value problems into initial value problems, iteratively adjusting initial conditions and integrating using methods like Runge-Kutta. Its effectiveness in solving complex flow models yields precise insights into fluid behavior. Consequently, we utilized this approach to address Equations (8)–(12). Shampine et al. [46] furnished a comprehensive description of Bvp4c. **Figure 2** shows the flow chart of the current investigation. Additionally, several new variables were introduced, outlined as follows:

$$\begin{aligned} f = p_1, f' = p_2, f'' = p_3, f''' = p_3', \\ \theta = p_4, \theta' = p_5, \theta'' = p_5', \\ \phi = p_6, \phi' = p_7, \phi'' = p_7', \\ \varphi = p_8, \varphi' = p_9, \varphi'' = p_9', \end{aligned} \tag{23}$$

$$p_3' = \frac{1}{\alpha(1+2\gamma\xi)[1+(2-\alpha)(\beta p_3)^{\alpha-1}]} \times [-\gamma[1+(2-\alpha)(\beta p_3)^{\alpha-1}]p_3 + [((1+\beta p_3)^{\alpha-1})^2]Mp_2 + [(1 + \beta p_3)^{\alpha-1})]^2\sigma_1 p_2 - [(1+\beta p_3)^{\alpha-1}]^2[p_1 p_3 - F_r(p_2)^2] - \aleph[p_4 - N_r p_6 - N_c p_8]] \tag{24}$$

$$p_5' = \frac{1}{\frac{4}{3}Rd[(1+(\theta_w-1)p_4)^3](1+2\gamma\xi)} \times [-4Rd(p_5)^2[(1+(\theta_w-1)p_4)^2(\theta_w-1)] - 2\gamma p_5 - N_b p_5 p_7 - N_t(p_5)^2 - Prp_1 p_5] \tag{25}$$

$$p_7' = -p_2 p_7 Le\frac{\xi}{2} - Lep_1 p_7 - \frac{N_t}{N_b}(p_5' + \gamma p_5) + Le\Omega(1+\Upsilon^* p_4)exp(\frac{-E}{1+\Upsilon^* p_4})p_6 \tag{26}$$

$$p_9' = -Le(p_1 p_9 + \xi p_2 p_8) - Pe[\sigma_1 p_7 - (\gamma\sigma_1 + p_8)p_7'] - Lep_9 p_6 \tag{27}$$

Together with the associated boundary conditions:

$$p_1(0) = 0,\ \ p_2(0) = 1,\ \ p_5(0) = -Bi[1-p_4(0)],\ \ \ p_7(0) + \frac{N_t}{N_b}p_5(0) = 0, \tag{28}$$

$$p_8(0) = 1,\ \ \text{at}\ \xi = 0$$

$$p_2 \to 0,\ \ p_4 \to 0,\ \ p_6 \to 0,\ \ p_8 \to 0,\ \ \text{at}\ \xi \to 0 \tag{29}$$

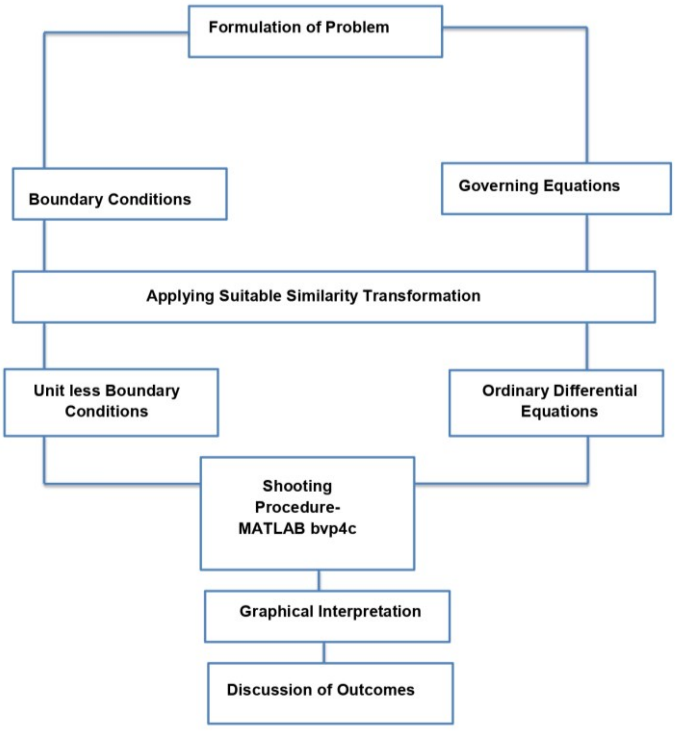

Figure 2. Flow chart for current problem.

5. Results and discussion

This part elucidates the graphs of physical characteristics such as distribution of velocity component $f'(\xi)$, distribution of temperature $\theta(\xi)$, distribution of concentration of nanoparticles $\phi(\xi)$, and distribution of motile oxytactic microorganisms $\chi(\xi)$. In the process of altering the physical variables of our interest, the variables left behind have been assigned these values $0.5 \leq M \leq 3.5$, $0.4 \leq Bi \leq 4.5$, $0.5 \leq Rd \leq 1$, $0.2 \leq \gamma \leq 0.8$, $m = 3$, $0 \leq \sigma_1 \leq 1$, $0.5 \leq \theta_w \leq 2$, $4 \leq Fr \leq 15$, $1 \leq \beta \leq 5$, $Pr = 1$ and $n = 1$.

5.1. Velocity profile

The persuasion of the slip parameter α, the magnetization factor M, the thermal radiation parameter Rd, the microorganism concentration difference constant Ω, and the parameter for buoyancy ratio Nr on the fluid speed $f'(\xi)$ is depicted in **Figure 3a–e**. The effects of the magnetization factor M on velocity graph $f'(\xi)$ is manifested in **Figure 3a**. A declining behaviour is prominent for velocity distribution by increasing the magnetization factor M. For higher values of (M = 0.5, 1.5, 2.5, 3.5), **Figure 3a** shows a decreasing trend of $f'(\xi)$. Because it depends on Lorentz force, the interparticle resistance increases as increases, which reduces $f'(\xi)$. The consequence of the slip parameter α on the velocity graph $f'(\xi)$ is shown in **Figure 3b**. By increasing α, an increase in velocity distribution is observed. Because, the presence of slip effectively increases the speed of particles in fluid. Similarly, the results for the radiation parameter Rd shown in **Figure 3c**. As the radiation constant Rd increases, the velocity distribution $f'(\xi)$ raises. Solar radiation can help in improving different heat and thermal moulding procedures in the twenty-first century. **Figure 3d** shows the effects of the microorganism concentration difference constant Ω. It is evident from the graph that there is a decline in velocity profile for changing values of Ω. The graphical results for the parameter for buoyancy ratio Nr is shown in **Figure 3(e)**. As the values of the parameter for buoyancy ratio Nr increases, the velocity distribution $f'(\xi)$ also shows an increasing trend.

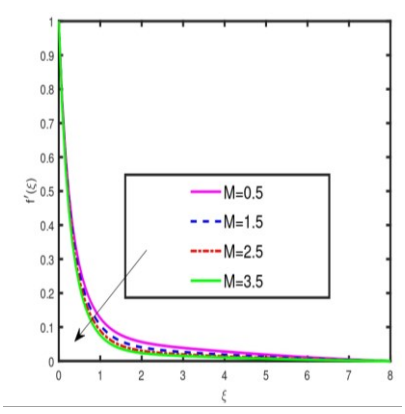

(a)

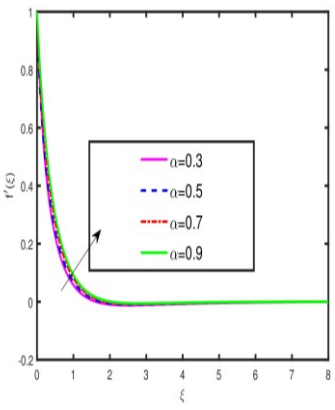

(b)

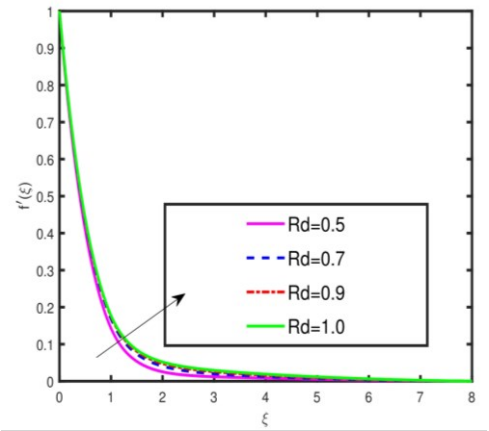

(c)

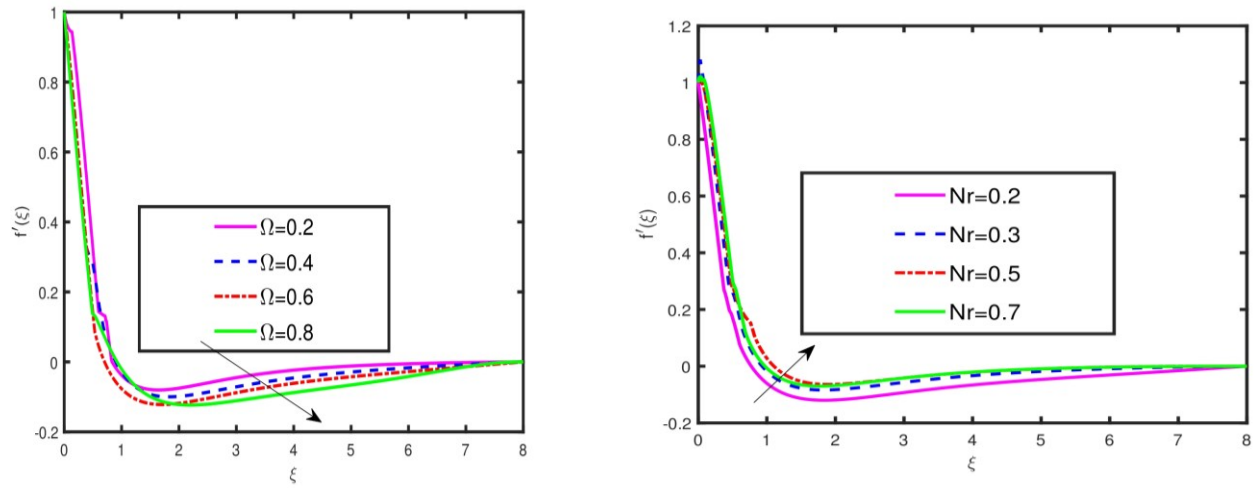

(d) **(e)**

Figure 3. Influence of **(a)** M; **(b)** α; **(c)** Rd; **(d)** Ω; **(e)** Nr on $f'(\xi)$.

5.2. Temperature distribution profile

The influences of the magnetization factor M, the thermal radiation parameter Rd, the thermophoresis parameter Nt, the curvature parameter γ and the bioconvention Peclet number Pe on the fluid speed $\theta(\xi)$ is shown in **Figure 4a–e**. Effects of the magnetization factor M on temperature field $\theta(\xi)$ is portrayed in **Figure 4a**. A declining behaviour is prominent for temperature distribution by increasing the magnetization factor M. For higher values of (M = 0.5, 1.5, 2.5, 3.5), **Figure 4a** shows a decreasing trend of $\theta(\xi)$. Because it depends on Lorentz force, the interparticle resistance increases as it increases, which reduces $\theta(\xi)$. The results for and the thermophoresis parameter Nt, as well as the thermal radiation parameter Rd is illustrated in **Figure 4b,c** respectively. For Nt, a declining behaviour of $\theta(\xi)$ observed in **Figure 4b**. The thermophoresis phenomenon is important in many processes because it involves migrating nanoparticles in a low temperature zone due to temperature differences. Similarly, the results for the radiation parameter Rd shown in **Figure 4c**. As the radiation constant Rd increases, the temperature distribution $\theta(\xi)$ changes. In **Figure 4d,e**, the effects of the bio convention Peclet number Pe and the curvature parameter γ are plotted. By altering Pe, a retarding behavior is discovered; this tendency establishes because Pe develop a reverse relationship with temperature field. $\theta(\xi)$ reduced as a result of this inverse relationship. **Figure 4e** demonstrates how the curvature parameter impacts the temperature profile of Ellis nanofluid. The temperature profile $\theta(\xi)$ decreases as the curvature parameter γ increases, leading to a reduction in the heat transfer rate.

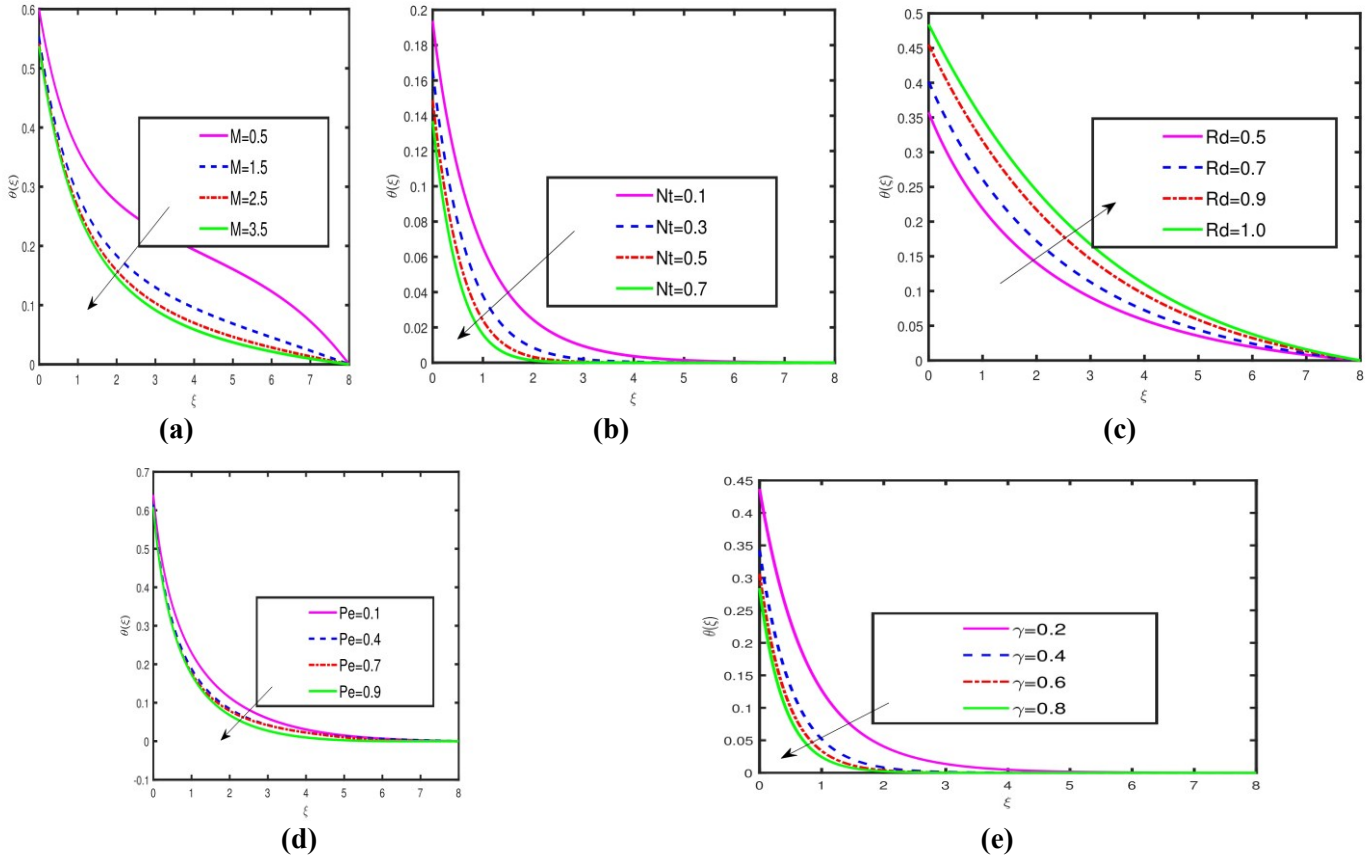

Figure 4. Influence of **(a)** M; (b) Nt; **(c)** Rd; **(d)** γ; **(e)** Pe on $\theta(\xi)$.

5.3. Concentration profile significance

To examine changes in profile for concentration of nanoparticles $\phi(\xi)$ opposite different values of magnetization factor M, the thermal radiation parameter Rd, the Brownian movement parameter Nb, Lewis number Le and the Forchheimer number Fr **Figure 5a–e** are made. Effects of the magnetization factor on $\phi(\xi)$ is displayed in **Figure 5a**. An increasing behaviour is prominent for $\phi(\xi)$ by increasing the magnetic parameter M. For higher values of (M = 0.5, 1.5, 2.5, 3.5), **Figure 5a** shows an increasing trend of $\phi(\xi)$. **Figure 5b** indicates how the effects on $\phi(\xi)$ on Ellis nanofluid increases as the amounts of the Fr rise. Similarly, the results for the radiation parameter Rd are shown in **Figure 5c**. As the radiation constant Rd increases, the temperature distribution $\phi(\xi)$ first increases then shows a declining trend. The ramifications of yet two other crucial parameters, the Lewis number Le and the Brownian movement parameter Nb are shown in **Figure 5d**,**e** respectively. Although the concentration of nanoparticles decreases with Le but for Nb the profile for concentration of nanoparticles improves.

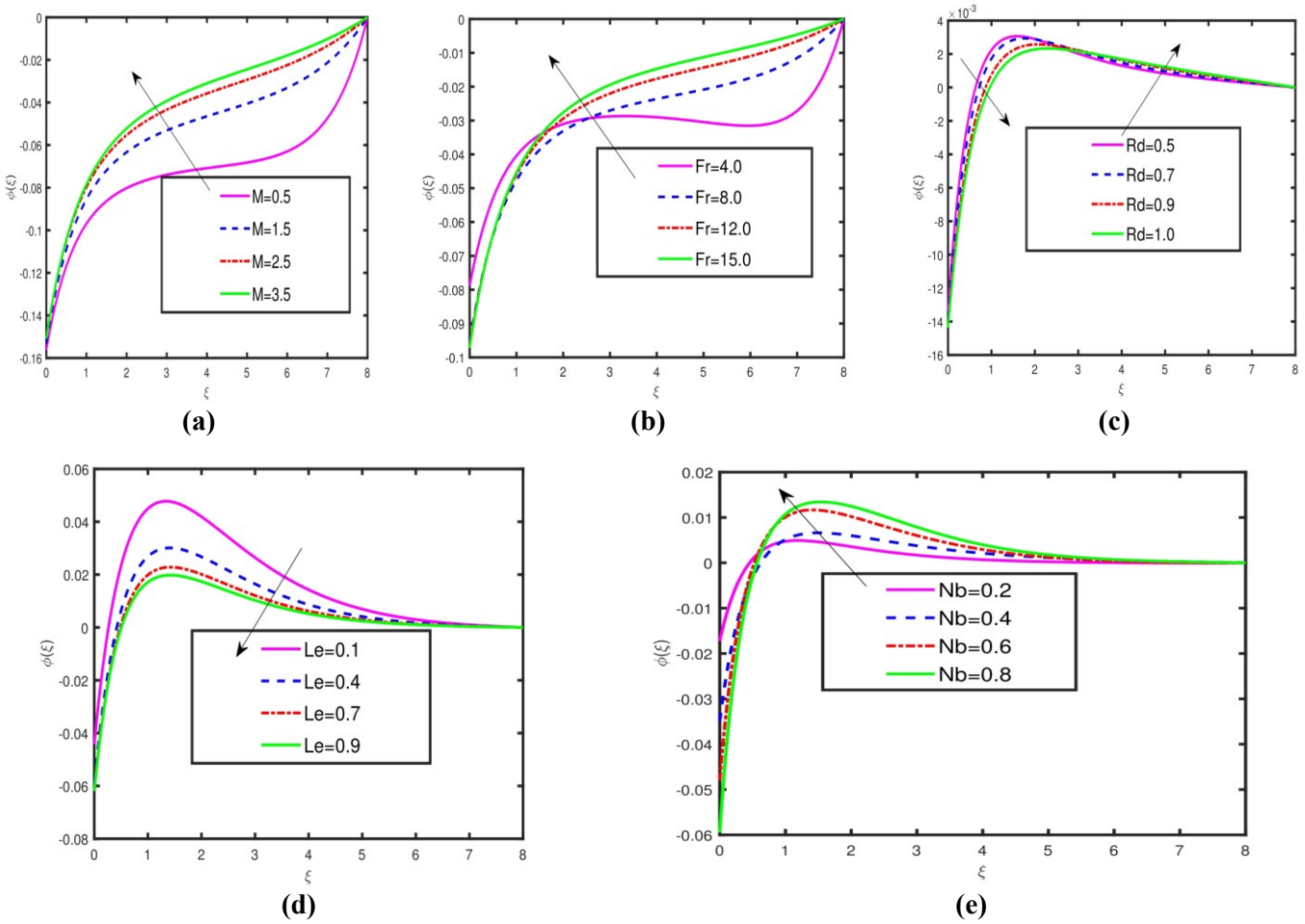

Figure 5. Influence of **(a)** M; **(b)** Fr; **(c)** Rd; **(d)** Le; **(e)** Nb on $\phi(\xi)$.

5.4. Density of motile microorganism profile

Figure 6a–e shows the changes in the profile for independently moving microorganisms $\chi(\xi)$ for various parameters such as thermal Biot number Bi, stretching parameter β, magnetization factor M, Prandtl number Pr and Lewis parameter Lb on profile for independently moving microorganism $\chi(\xi)$. **Figure 6a** is prepared to depict the physical impact caused by thermal Biot number Bi on $\chi(\xi)$. It is easy to observe that $\chi(\xi)$ is a decreasing function of (Bi= 0.4, 1.5, 3.0, 4.5). As thermal Biot number has a connection to the coefficient of heat transfer, that causes a decrease in the independently moving microorganisms $\chi(\xi)$. An increasing behaviour is prominant for $\chi(\xi)$ by increasing the magnetic parameter M. For higher values of (M = 0.5, 1.5, 2.5, 3.5), **Figure 6b** shows an increasing trend of $\chi(\xi)$. The stretching parameter β for the dimensionless independently moving microorganisms $\chi(\xi)$ is graphed in **Figure 6c**. The profile for independently moving microorganisms $\chi(\xi)$ decreases as β increased. **Figures 6d,e** are prepared to depict the physical impact caused by Pr and Lb on independently moving microorganisms $\chi(\xi)$. It is easy to observe that $\chi(\xi)$ is a decreasing function of (Pr = 10, 12, 14, 16). Further, a distinguishing motile microorganism profile $\chi(\xi)$ is found when the value of Lb increases. The physical reasoning is that a bigger deviation in Lb is connected with reduced motility of motile bacteria, which decays $\chi(\xi)$ as a result of this.

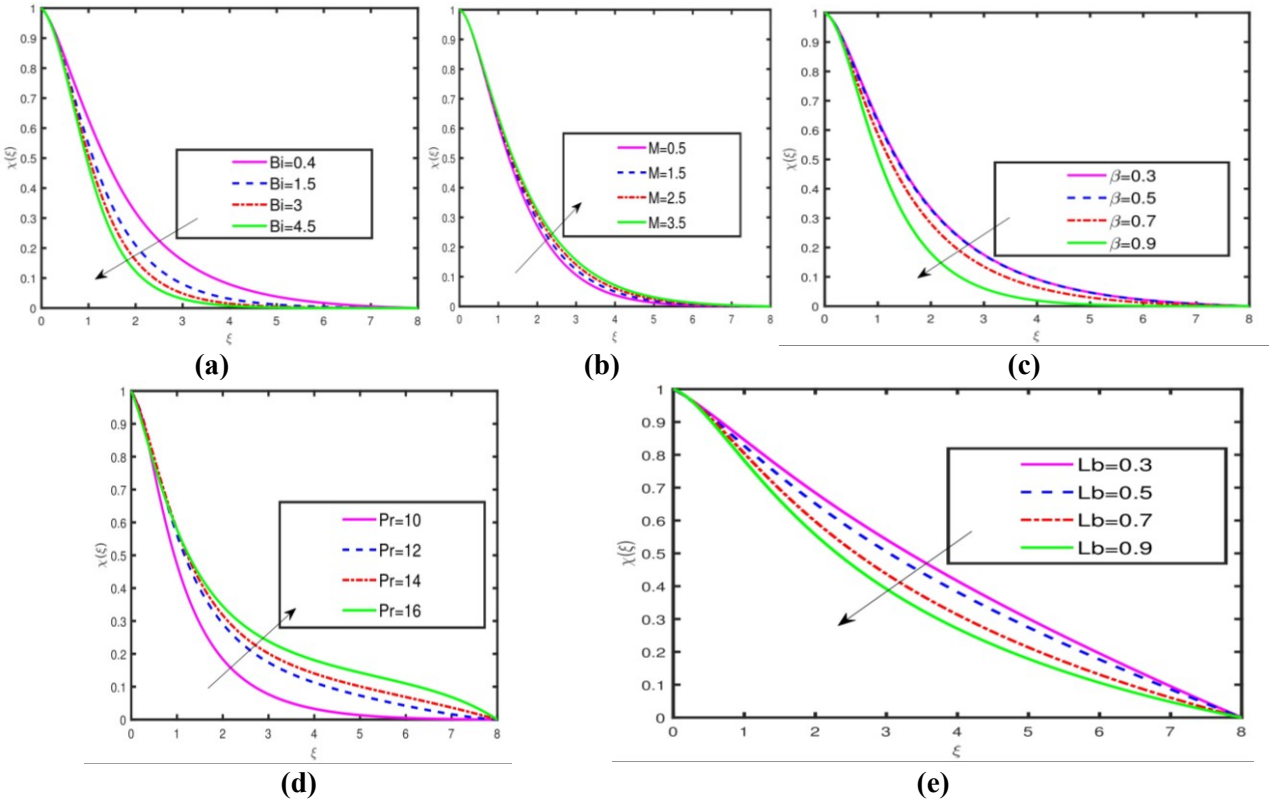

Figure 6. Influence of **(a)** *Bi*; **(b)** *M*; **(c)** β; **(d)** *Pr*; **(e)** *Lb* on $\chi(\xi)$.

5.5. Streamlines patterns in Ellis nanofluid flow

This subsection illustrates the streamlines for the mixed convection parameter and slip parameter, as shown in **Figure 7a–d**. The graphs demonstrate the significant impact of both the mixed convection parameter ℵand the slip parameter α on fluid dynamics. When $\aleph = 0.7$ the streamlines are densely packed near the surface, indicating a sharper velocity gradient and stronger convective flow due to buoyancy forces. In contrast, a lower mixed convection value $\aleph = 0.2$ results in smoother, less curved streamlines, highlighting the dominance of viscous forces. Regarding the slip parameter α, increasing it from 1.5 to 2.5 reduces boundary layer thickness and curvature of the streamlines, suggesting less friction and shear stress at the boundary, which enhances flow efficiency. This effect is particularly beneficial for applications like microfluidics, where minimizing drag is crucial. Conversely, lower α values result in thicker boundary layers and greater resistance, slowing down the fluid flow (see **Figure 7c,d**). Overall, mixed convection controls the intensity of surface flow, while the slip parameter governs flow resistance, both essential for optimizing fluid dynamics in systems that require precise control, such as microfluidic devices.

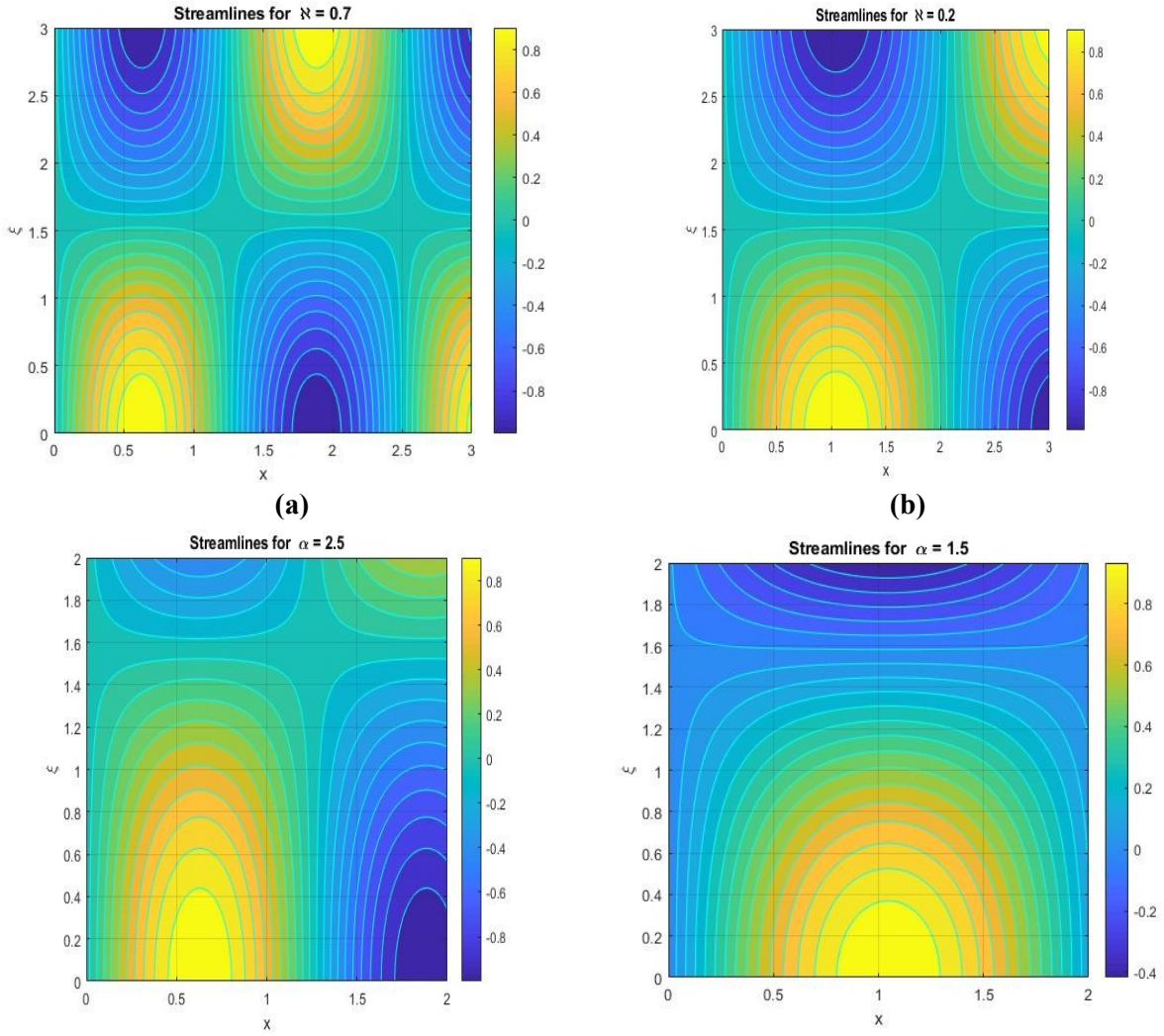

Figure 7. Streamlines for **(a)** ℵ = 0.7, **(b)** ℵ = 0.2, **(c)** α = 2.5, **(d)** α = 1.5.

5.6. Isotherm patterns in Ellis nanofluid flow

The isotherm patterns depicted in **Figure 8a–d** offer profound insights into the thermal dynamics of Ellis nanofluid flow, particularly with respect to the Ellis fluid parameter β and porosity parameter σ_1. In **Figure 8a**, where ($\beta = 0.7$), the closely packed isotherms near the center indicate a steeper temperature gradient, signifying enhanced heat transfer and thermal conduction within the fluid. On the other hand, **Figure 8b**, with a lower ($\beta = 0.5$), shows more widely spaced isotherms, suggesting a gentler temperature gradient and reduced heat conduction, which reflects a decline in thermal efficiency. Focusing on the porosity parameter, **Figure 8c** illustrates that a higher ($\sigma_1 = 1.5$) results in a well-structured, periodic isotherm pattern, promoting more effective thermal dissipation throughout the fluid. In contrast, **Figure 8d**, where ($\sigma_1 = 1.1$), reveals elongated and less organized isotherms, indicating diminished heat transfer efficiency due to increased thermal resistance at the boundaries. These findings highlight the critical roles of elevated β and σ_1 values in optimizing heat conduction and distribution within the Ellis nanofluid flow.

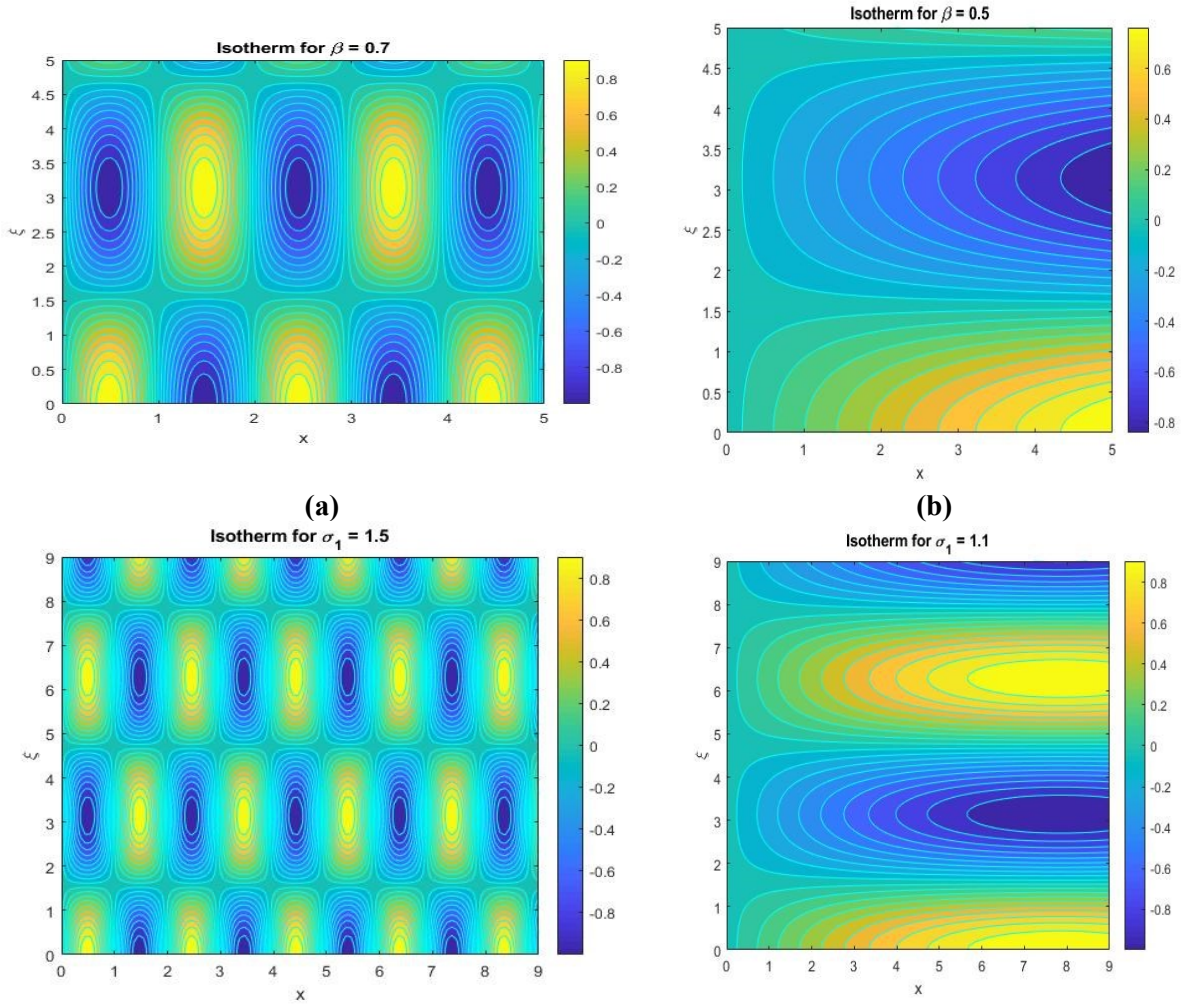

Figure 8. Isotherms for **(a)** $\beta = 0.7$, **(b)** $\beta = 0.5$, **(c)** $\sigma_1 = 1.5$, **(d)** $\sigma_1 = 1.1$.

5.7. Tabular discussion and validation

To validate this research, we compared the skin friction values with those reported by Rooman et al. [47] and Awan et al. [44] under specific conditions where M varies and all other parameters are set to zero, ensuring optimal heat and mass transfer in our model. The results demonstrate excellent agreement with existing literature (see **Table 1**).

Table 1. A comparison of $f'(0)$ for different inputs of M.

M	Rooman et al. [47]	Awan et al. [44]	Current result
0.0	−0.821821	−0.8266554	−0.8267556
0.4	−0.924421	−0.9186823	−0.9286826
0.8	−1.018311	−1.0488087	−1.0588092

6. Conclusion

Numerical analysis was conducted to explore the steady mixed convection of Ellis nano-liquid flow over a stretching cylinder, incorporating Darcy-Forchheimer

and nonlinear thermal radiation effects. The numerical solution of this model involves formulating a system of partial differential equations, which is subsequently computed by utilizing the bvp4c function available in MATLAB. The acquired outcomes are visually presented and analyzed. The following observations have been made after a thorough examination of the problem:

- Increasing the magnetization factor M results in a decreasing velocity profile $f'(\xi)$ due to the stronger Lorentz force increasing interparticle resistance.
- An augmentation in the Peclet number (Pe) and thermophoresis value results in a decline in the thermal layer.
- The Ellis fluid parameter β results in a decrease in the motile density profile $\chi(\xi)$.
- Brownian motion enhances the thermal profile, while saturation in thermophoresis values leads to a decrease in flow.
- It has been uncovered that an increased approximation of the Forchheimer number results in an enlargement of the concentration profile $\phi(\xi)$.
- Our study demonstrates that varying the radiation parameter (Rd) provides valuable insights into the behavior of Ellis nanofluids under magnetized bioconvective conditions, emphasizing the significance of considering multiple factors for a comprehensive understanding of the fluid dynamics.
- Lower mixed convection values allow viscous forces to dominate, leading to smoother, less curved streamlines.
- Increased porosity parameter σ_1 values produce well-structured isotherms, promoting efficient thermal dissipation throughout the fluid.

Future research in this domain should explore the ramification of variable activation energy on the behavior of oxytactic microorganisms within magnetized bioconvective Ellis nanofluids, alongside extending studies to three-dimensional systems for a more comprehensive understanding. Experimental validation is essential to enhance credibility, while investigating additional dissipative processes like thermal diffusion could provide deeper insights. Further applications in bioengineering and materials science should be explored, considering the impact of external fields and conducting optimization studies to maximize efficiency in practical applications. These endeavors would significantly advance the understanding and application of magnetized bioconvective Ellis nanofluids.

Author contributions: Methodology, TA; software, TA; validation, MA; formal analysis, TA, MA and MC; investigation, TA, MMA and MI; data curation, MMA; writing—original draft preparation, TA and MMA; writing—review and editing, TA, MA, MC and MI; visualization, MA; supervision, MMA and MI. All authors have read and agreed to the published version of the manuscript.

Acknowledgments: The authors express gratitude to the reviewers for their valuable suggestions and comments, contributing to the enhanced clarity of this manuscript.

Conflict of interest: The authors declare no conflict of interest.

Nomenclature

$\bar{r}, \bar{z}$: Cylinderical coordinates (-)
$\bar{u}$: Velocity component along horizontal axis (z-axis) $(\mathrm{m/s})$
$\bar{w}$: Velocity component along radial axis (r-axis) $(\mathrm{m/s})$
$\bar{T}$: Temperature of particles (K)
k: Nanofuid thermal conductivity $(\mathrm{W/mK})$
M: Magnetic parameter (-)
$\bar{C}$: Concentration of particles $(\mathrm{mol/m^3})$
$\bar{N}$: Microorganism's density (-)
T_w: Surface temperature $((T)$
F_r: Forchheimer number (-)
C_w: Surface concentration (mol/m^3)
Rd: Thermal radiation parameter (-)
N_w: Surface microorganisms (-)
Bi: Thermal Biot number (-)
Pr: Prandtl number (-)
N_r: Parameter of buoyancy force $(-)$
N_c: Bioconvection Rayleigh number $(-)$
G_{rt}: Grashof number $(-)$
T_∞: Ambient temperature (-)
C_∞: Free stream concentration $(\mathrm{mol/m^3})$
N_∞: Ambient microorganisms (-)
Re_x: Local Reynolds number (-)
D_m: Microorganism's difusion coefcient (-)
E: Activation energy parameter (-)
N_t: Thermophoresis parameter (-)
Le: Lewis number (-)
Lb: Bioconvection Lewis number (-)
D_B: Brownian motion coefcient $(\mathrm{m^2/s})$

Greek symbols

γ: Curvature parameter (-)
ν: Kinematic viscosity $(\mathrm{m^2/s})$
β: Ellis Fluid parameters (-)
μ: Dynamic viscosity $(\mathrm{g/ms})$
σ_1: Porosity parameters (-)
θ_w: Temperature ratio parameter (-)
Ω: Coefficient of chemical reaction (-)
α: Slip parameter (-)
ρ_f: Density of the fluid $(\mathrm{kg/m^3})$
δ_1: Bacterial concentration parameter (-)

References

1. Turkyilmazoglu M. MHD natural convection in saturated porous media with heat generation/absorption and thermal

radiation: closed-form solutions. Archives of Mechanics. 2019; 71(1): 49-64. doi: 10.24423/aom.3049
2. Turkyilmazoglu M. Flow of nanofluid plane wall jet and heat transfer. European Journal of Mechanics - B/Fluids. 2016; 59: 18-24. doi: 10.1016/j.euromechflu.2016.04.007
3. Arafa AAM, Ahmed SE, Allan MM. Peristaltic flow of non-homogeneous nanofluids through variable porosity and heat generating porous media with viscous dissipation: Entropy analyses. Case Studies in Thermal Engineering. 2022; 32: 101882. doi: 10.1016/j.csite.2022.101882
4. Hussain F, Nazeer M, Ghafoor I, et al. Perturbation solution of Couette flow of Casson nanofluid with composite porous medium inside a vertical channel. Nanoscience and Technology: An International Journal. 2022; 13(4): 23-44. doi: 10.1615/nanoscitechnolintj.2022038799
5. Abbas N, Shatanawi W, shatnawi TAM. Thermodynamic study of radiative chemically reactive flow of induced MHD sutterby nanofluid over a nonlinear stretching cylinder. Alexandria Engineering Journal. 2023; 70: 179-189. doi: 10.1016/j.aej.2023.02.038
6. Nadeem S, Khan MN, Abbas N. Transportation of slip effects on nanomaterial micropolar fluid flow over exponentially stretching. Alexandria Engineering Journal. 2020; 59(5): 3443-3450. doi: 10.1016/j.aej.2020.05.024
7. Amjad M, Zehra I, Nadeem S, et al. Influence of Lorentz force and Induced Magnetic Field Effects on Casson Micropolar nanofluid flow over a permeable curved stretching/shrinking surface under the stagnation region. Surfaces and Interfaces. 2020; 21: 100766. doi: 10.1016/j.surfin.2020.100766
8. Ramesh K, Mebarek-Oudina F, Souayeh B. Mathematical Modelling of Fluid Dynamics and Nanofluids. CRC Press; 2023. doi: 10.1201/9781003299608
9. Yahya AU, Salamat N, Huang WH, et al. Thermal charactristics for the flow of Williamson hybrid nanofluid (MoS_2 + ZnO) based with engine oil over a streched sheet. Case Studies in Thermal Engineering. 2021; 26: 101196. doi: 10.1016/j.csite.2021.101196
10. Ahmad F, Abdal S, Ayed H, et al. The improved thermal efficiency of Maxwell hybrid nanofluid comprising of graphene oxide plus silver / kerosene oil over stretching sheet. Case Studies in Thermal Engineering. 2021; 27: 101257. doi: 10.1016/j.csite.2021.101257
11. Gul T, Ahmed Z, Jawad M, et al. Bio-convectional Nanofluid Flow Due to the Thermophoresis and Gyrotactic Microorganism Between the Gap of a Disk and Cone. Brazilian Journal of Physics. 2021; 51(3): 687-697. doi: 10.1007/s13538-021-00888-6
12. Abdal S, Hussain S, Siddique I, et al. On solution existence of MHD Casson nanofluid transportation across an extending cylinder through porous media and evaluation of priori bounds. Scientific Reports. 2021; 11(1). doi: 10.1038/s41598-021-86953-1
13. Narahari M, Sreenadh S, Arunachalam PV. Peristaltic pumping flow of an-Ellis fluid through a circular tube. Bulletin of Pure & Applied Sciences. 2000; 19(1): 493-503.
14. Steller RT. Generalized slit flow of an ellis fluid. Polymer Engineering & Science. 2001; 41(11): 1859-1870. doi: 10.1002/pen.10883
15. Ali N, Abbasi A, Ahmad I. Channel flow of Ellis fluid due to peristalsis. AIP Advances. 2015; 5(9). doi: 10.1063/1.4932042
16. Goud JS, Reddy RH. Peristaltic motion of an Ellis fluid model in a vertical uniform tube with wall properties. International Journal of Civil Engineering and Technology. 2018; 9(1): 847-856.
17. Shaheen N, Alshehri HM, Ramzan M, et al. Soret and Dufour effects on a Casson nanofluid flow past a deformable cylinder with variable characteristics and Arrhenius activation energy. Scientific Reports. 2021; 11(1). doi: 10.1038/s41598-021-98898-6
18. Hayat T, Shafiq A, Alsaedi A. MHD axisymmetric flow of third grade fluid by a stretching cylinder. Alexandria Engineering Journal. 2015; 54(2): 205-212. doi: 10.1016/j.aej.2015.03.013
19. Grigoriadis DGE, Sarris IE, Kassinos SC. MHD flow past a circular cylinder using the immersed boundary method. Computers & Fluids. 2010; 39(2): 345-358. doi: 10.1016/j.compfluid.2009.09.012
20. Anuar NS, Bachok N, Turkyilmazoglu M, et al. Analytical and stability analysis of MHD flow past a nonlinearly deforming vertical surface in Carbon Nanotubes. Alexandria Engineering Journal. 2020; 59(1): 497-507. doi: 10.1016/j.aej.2020.01.024
21. Ramesh K, Mebarek-Oudina F, Ismail AI, et al. Computational analysis on radiative non-Newtonian Carreau nanofluid flow in a microchannel under the magnetic properties. Scientia Iranica. 2023; 30(2): 376-390. doi: 10.24200/sci.2022.58629.5822
22. Mebarek-Oudina F, Dharmaiah G, Balamurugan KS, et al. The Role of Quadratic-Linearly Radiating Heat Source with

Carreau Nanofluid and Exponential Space-Dependent Past a Cone and a Wedge: A Medical Engineering Application and Renewable Energy. Journal of Computational Biophysics and Chemistry. 2023; 22(08): 997-1011. doi: 10.1142/s2737416523420073

23. Khan JA, Mustafa M. A numerical analysis for non-linear radiation in MHD flow around a cylindrical surface with chemically reactive species. Results in Physics. 2018; 8: 963-970. doi: 10.1016/j.rinp.2017.12.067
24. Kuznetsov AV, Avramenko AA. Effect of small particles on this stability of bioconvection in a suspension of gyrotactic microorganisms in a layer of finite depth. International Communications in Heat and Mass Transfer. 2004; 31(1): 1-10. doi: 10.1016/S0735-1933(03)00196-9
25. Geng P, Kuznetsov AV. Settling of bidispersed small solid particles in a dilute suspension containing gyrotactic micro-organisms. International Journal of Engineering Science. 2005; 43(11-12): 992-1010. doi: 10.1016/j.ijengsci.2005.03.002
26. Kuznetsov AV. Non-oscillatory and oscillatory nanofluid bio-thermal convection in a horizontal layer of finite depth. European Journal of Mechanics - B/Fluids. 2011; 30(2): 156-165. doi: 10.1016/j.euromechflu.2010.10.007
27. Bég OA, Prasad VR, Vasu B. Numerical Study of Mixed Bioconvection in Porous Media Saturated with Nanofluid Containing Oxytactic Microorganisms. Journal of Mechanics in Medicine and Biology. 2013; 13(04): 1350067. doi: 10.1142/s021951941350067x
28. Mebarek-Oudina F, Chabani I, Vaidya H, et al. Hybrid-nanofluid magneto-convective flow and porous media contribution to entropy generation. International Journal of Numerical Methods for Heat & Fluid Flow. 2024; 34(2): 809-836. doi: 10.1108/hff-06-2023-0326
29. Dharmaiah G, Mebarek-Oudina F, Balamurugan KS, et al. Numerical Analysis of the Magnetic Dipole Effect on a Radiative Ferromagnetic Liquid Flowing over a Porous Stretched Sheet. Fluid Dynamics & Materials Processing. 2024; 20(2): 293-310. doi: 10.32604/fdmp.2023.030325
30. Akbar NS. Bioconvection peristaltic flow in an asymmetric channel filled by nanofluid containing gyrotactic microorganism. International Journal of Numerical Methods for Heat & Fluid Flow. 2015; 25(2): 214-224. doi: 10.1108/hff-07-2013-0242
31. Bhatti MM, Zeeshan A, Ellahi R. Simultaneous effects of coagulation and variable magnetic field on peristaltically induced motion of Jeffrey nanofluid containing gyrotactic microorganism. Microvascular Research. 2017; 110: 32-42. doi: 10.1016/j.mvr.2016.11.007
32. Dharmaiah G, Mebarek-Oudina F, Rama Prasad JL, et al. Exploration of bio-convection for slippery two-phase Maxwell nanofluid past a vertical induced magnetic stretching regime associated for biotechnology and engineering. Journal of Molecular Liquids. 2023; 391: 123408. doi: 10.1016/j.molliq.2023.123408
33. Abbas IA, Palani G. Effects of magnetohydrodynamic flow past a vertical plate with variable surface temperature. Applied Mathematics and Mechanics. 2010; 31(3): 329-338. doi: 10.1007/s10483-010-0306-9
34. Chakraborty T, Das K, Kundu PK. Framing the impact of external magnetic field on bioconvection of a nanofluid flow containing gyrotactic microorganisms with convective boundary conditions. Alexandria Engineering Journal. 2018; 57(1): 61-71. doi: 10.1016/j.aej.2016.11.011
35. Umar M, Akhtar R, Sabir Z, et al. Numerical Treatment for the Three-Dimensional Eyring-Powell Fluid Flow over a Stretching Sheet with Velocity Slip and Activation Energy. Advances in Mathematical Physics. 2019; 2019: 1-12. doi: 10.1155/2019/9860471
36. Khan SU, Rauf A, Shehzad SA, et al. Study of bioconvection flow in Oldroyd-B nanofluid with motile organisms and effective Prandtl approach. Physica A: Statistical Mechanics and its Applications. 2019; 527: 121179. doi: 10.1016/j.physa.2019.121179
37. Akolade MT, Akhtar T, Awad MM, et al. Bioconvection analysis of EMHD and dissipative Williamson nanofluid over a three dimensional Riga plate with Joule heating effect. International Journal of Modelling and Simulation. 2023: 1-13. doi: 10.1080/02286203.2023.2265524
38. Waqas H, Khan SU, Shehzad SA, et al. Radiative flow of Maxwell nanofluid containing gyrotactic microorganism and energy activation with convective Nield conditions. Heat Transfer—Asian Research. 2019; 48(5): 1663-1687. doi: 10.1002/htj.21451
39. Waqas H, Khan SU, Tlili I, et al. Significance of Bioconvective and Thermally Dissipation Flow of Viscoelastic Nanoparticles with Activation Energy Features: Novel Biofuels Significance. Symmetry. 2020; 12(2): 214. doi: 10.3390/sym12020214
40. Shahid A, Zhou Z, Hassan M, et al. Computational Study of Magnetized Blood Flow in The Presence of Gyrotactic

Microorganisms Propelled Through a Permeable Capillary in A Stretching Motion. International Journal for Multiscale Computational Engineering. 2018; 16(5): 409-426. doi: 10.1615/intjmultcompeng.2018026030

41. Waqas H, Khan SU, Hassan M, et al. Analysis on the bioconvection flow of modified second-grade nanofluid containing gyrotactic microorganisms and nanoparticles. Journal of Molecular Liquids. 2019; 291: 111231. doi: 10.1016/j.molliq.2019.111231
42. Hiba B, Redouane F, Jamshed W, et al. A novel case study of thermal and streamline analysis in a grooved enclosure filled with (Ag–MgO/Water) hybrid nanofluid: Galerkin FEM. Case Studies in Thermal Engineering. 2021; 28: 101372. doi: 10.1016/j.csite.2021.101372
43. Sharif MAR, Mohammad TR. Natural convection in cavities with constant flux heating at the bottom wall and isothermal cooling from the sidewalls. International Journal of Thermal Sciences. 2005; 44(9): 865-878. doi: 10.1016/j.ijthermalsci.2005.02.006
44. Awan AU, Ali B, Shah SAA, et al. Numerical analysis of heat transfer in Ellis hybrid nanofluid flow subject to a stretching cylinder. Case Studies in Thermal Engineering. 2023; 49: 103222. doi: 10.1016/j.csite.2023.103222
45. Alwatban AM, Khan SU, Waqas H, et al. Interaction of Wu's Slip Features in Bioconvection of Eyring Powell Nanoparticles with Activation Energy. Processes. 2019; 7(11): 859. doi: 10.3390/pr7110859
46. Shampine LF, Kierzenka J, Reichelt MW. Solving boundary value problems for ordinary differential equations in MATLAB with bvp4c. Tutorial Notes. 2000; 1-27.
47. Rooman M, Jan MA, Shah Z, et al. Entropy generation and nonlinear thermal radiation analysis on axisymmetric MHD Ellis nanofluid over a horizontally permeable stretching cylinder. Waves in Random and Complex Media. 2022: 1-15. doi: 10.1080/17455030.2021.2020934